

**High critical-current density with less anisotropy in $\text{BaFe}_2(\text{As,P})_2$
epitaxial thin films: Effect of intentionally grown c -axis vortex-pinning centers**

Hikaru Sato¹, Hidenori Hiramatsu^{1,2}, Toshio Kamiya^{1,2}, and Hideo Hosono^{1,2,3*}

1: *Materials and Structures Laboratory, Tokyo Institute of Technology, Mailbox R3-1, 4259 Nagatsuta-cho, Midori-ku, Yokohama 226-8503, Japan*

2: *Materials Research Center for Element Strategy, Tokyo Institute of Technology, Mailbox S2-16, 4259 Nagatsuta-cho, Midori-ku, Yokohama 226-8503, Japan*

3: *Frontier Research Center, Tokyo Institute of Technology, Mailbox S2-13, 4259 Nagatsuta-cho, Midori-ku, Yokohama 226-8503, Japan*

PACS numbers: 74.70.Xa (Superconducting materials: pnictides), 74.78.-w (Superconducting films), 74.25.F- (Superconductors: transport properties)

Abstract

We report herein a high and isotropic critical-current density J_c for $\text{BaFe}_2(\text{As,P})_2$ epitaxial films. The isotropy of J_c with respect to the magnetic-field direction was improved significantly by decreasing the film growth rate to 2.2 Å/s. The low growth rate served to preferentially align dislocations along the c -axis, which work well as c -axis vortex-pinning centers. Because of the intentional introduction of effective pinning, the absolute J_c at 9 T was larger than that obtained for other iron-based superconductors and conventional alloy superconducting wires.

Footnote:

*: Author to whom correspondence should be addressed. Electronic mail:
hosono@mssl.titech.ac.jp

Iron-based superconductors,^[1] with their high critical temperature (T_c) up to 55 K^[2] and high upper critical field (H_{c2}) up to 100 T,^[3] are seen as new candidate materials for high-magnetic-field applications such as superconducting wires and tapes. In particular, 122-type $\text{Ba}(\text{Fe}_{1-x}\text{Co}_x)_2\text{As}_2$ ($\text{BaFe}_2\text{As}_2:\text{Co}$) has been found to have attractive properties such as a large H_{c2} of over 50 T, a small anisotropy factor ($\gamma = 1$ to 2),^[4] and an advantageous grain-boundary nature.^[5] Thus, of the iron-based superconductor thin films, $\text{BaFe}_2\text{As}_2:\text{Co}$ epitaxial films have been investigated most intensively, and their self-field critical-current density J_c is currently far above 1 MA/cm².^[6]

However, as compared to $\text{BaFe}_2\text{As}_2:\text{Co}$, 122-type $\text{BaFe}_2(\text{As}_{1-x}\text{P}_x)_2$ ($\text{BaFe}_2\text{As}_2:\text{P}$) exhibits a higher T_c (~ 31 K) and a comparable γ .^[7] In addition, it was recently reported^[8] that $\text{BaFe}_2\text{As}_2:\text{P}$ epitaxial films have a very high J_c of 10 MA/cm², which is two to three times greater than that of $\text{BaFe}_2\text{As}_2:\text{Co}$.^[9,10] Unfortunately, the decay rate of J_c for a $\text{BaFe}_2\text{As}_2:\text{P}$ epitaxial film under a magnetic field^[7] is greater than that of a $\text{BaFe}_2\text{As}_2:\text{Co}$ epitaxial film.^[11] This observation is attributed to the weak vortex pinning in $\text{BaFe}_2\text{As}_2:\text{P}$ because an isovalent P dopant is not thought to work as an effective pinning center.^[12,13] This characteristic contrasts sharply with $\text{BaFe}_2\text{As}_2:\text{Co}$, in which the disorder of aliovalent Co dopants in the Fe layers works as intrinsic vortex pinning centers. Therefore, to exploit the advantages of $\text{BaFe}_2\text{As}_2:\text{P}$ films, it is vital to enhance their vortex pinning so that a high J_c can be maintained under high magnetic fields.

Another important issue for wire/tape applications is the anisotropy of J_c . Since high- T_c superconductors such as cuprates and 1111-type iron-based superconductors have distinct layered structures, H_{c2} with $H // ab$ is higher than H_{c2} with $H // c$ because of their electronic anisotropy; their J_c properties also reflect this intrinsic

crystallographic anisotropy. Therefore, introducing pinning centers along the c -axis is a practical way to reduce their anisotropy.^[14,15] Heavy-ion irradiation experiments have clarified the attractive properties of iron-based superconductors, which are totally different from cuprates; introducing a high density of nanosize columnar defects does not degrade T_c until the dose-matching field becomes 21 T, which indicates the excellent potential of iron-based superconductors for high-field applications.^[16] Although these results revealed the high potential of iron-based superconductors if pinning centers as structural defects are introduced, it is difficult to apply to large-scale superconducting wires and tapes. Therefore, a simple fabrication process, which controls the shape, size, and density of defects, is more practical than introducing artificial pinning centers.

In the present study, we obtained a large isotropic J_c in BaFe₂As₂:P epitaxial films grown by high-temperature pulsed-laser deposition (PLD) at 1050 °C. The results indicated that the characteristics of vortex pinning depend largely on growth rate, which affects the structure of microscopic defects in the epitaxial films.

BaFe₂As₂:P films of 150–200 nm thickness were grown on MgO (001) single-crystal substrates by PLD. Optimally P-doped polycrystalline BaFe₂(As_{0.7}P_{0.3})₂ disks were used as the PLD targets, which were synthesized by a solid-state reaction of BaAs + 0.4Fe₂As + 0.6Fe₂P → BaFe₂(As_{0.7}P_{0.3})₂ at 930 °C for 16 h in a sealed Ar-filled stainless-steel tube. The pulsed-laser excitation source was the second harmonic of an Nd:YAG laser (wavelength = 532 nm, repetition rate = 10 Hz, laser fluence ~ 3 J/cm²). The base pressure of the growth chamber was approximately 5×10^{-7} Pa. Instead of a halogen-lamp heater,^[17] a semiconductor infrared laser diode was used (wavelength =

975 nm, maximum power = 300 W) to achieve high substrate temperatures (T_s) up to 1400 °C. The T_s was calibrated by an *ex-situ* measurement using a thermocouple connected to a substrate directly. To heat the substrate, a Mo plate was tightly contacted to the backside of the substrate and heated by focused infrared light, which provided uniform T_s over the substrate. First, we varied T_s from 700 to 1300 °C by maintaining similar growth rates of ~ 3 Å/s, which is almost the same as that used for the epitaxial growth of BaFe₂As₂:Co.^[17] After finding the optimum T_s , the growth rate was varied from 2.1 to 3.9 Å/s by changing the substrate–target distance.

To determine the crystalline phases and the small amount of impurity phases, θ -coupled 2θ -scan x-ray diffraction measurements (XRD, anode radiation: Cu K α) were performed with a high-power conventional XRD apparatus. The crystallinity of the epitaxial films was characterized on the basis of full widths at half maximum (FWHM) of the out-of-plane (2θ -fixed ω scans) rocking curves ($\Delta\omega$) of 002 diffraction and the in-plane ($2\theta_\chi$ -fixed ϕ scans) rocking curves ($\Delta\phi$) of 200 diffraction with a high-resolution XRD apparatus [HR-XRD, CuK α_1 monochromated by Ge (220)]. The chemical composition was determined from electron-probe microanalyzer (EPMA). For quantitative analyses, we employed the atomic number, absorption, fluorescence (ZAF) correction method using the following standard samples; BaTiO₃ for Ba, Fe for Fe, LaAs for As, and InP for P, which provided reasonable results as will be shown later (for a BaFe₂As₂:P film grown at an optimum $T_s \sim 1050$ °C, Ba: Fe: (As + P) = 1: 2.1 : 2.0).

The surface morphology was observed with an atomic force microscope (AFM). Cross-sectional microstructural images were obtained by scanning transmission electron

microscopy (STEM). The variation in chemical composition around defects was measured using energy-dispersive x-ray spectroscopy (EDXS) with a spatial resolution of about 1 nm. These characterizations were performed at room temperature.

Temperature (T) dependence of electrical resistivity (ρ) was measured by the four-probe method using Au electrodes with a physical property measurement system. To examine the transport properties of J_c , the films were patterned into microbridges by photolithography and an Ar milling process. The transport J_c was determined from voltage–current curves with the criterion of 1 $\mu\text{V}/\text{cm}$ under an external magnetic field (H) of up to 9 T. The angle θ_H of the applied H was varied from -30 to 120° (0 and 90° corresponding to $H // c$ -axis normal to the film surface and $H // ab$ plane, respectively).

Figure 1(a) summarizes the relationship between the growth condition (T_s and laser fluence) and crystallographic orientation of $\text{BaFe}_2\text{As}_2:\text{P}$ thin films grown at growth rates of $\sim 3 \text{ \AA}/\text{s}$. When $T_s \leq 950 \text{ }^\circ\text{C}$ [“Random oriented” region: triangles in Fig. 1(a) and lower XRD pattern in Fig. 1(b)], the films were preferentially oriented along the c -axis along with a smaller portion of nonoriented $\text{BaFe}_2\text{As}_2:\text{P}$ crystallites and Fe impurities appeared. When T_s was increased to $1100 \text{ }^\circ\text{C}$ [“Epitaxial” region: circles in Fig. 1(a)], epitaxial $\text{BaFe}_2\text{As}_2:\text{P}$ films were obtained; that is, only $00l$ diffractions were observed out of plane [middle row of Fig. 1(b)], and due to the tetragonal lattice, a clear four-fold symmetry was observed in the in-plane ϕ scan [Fig. 1(c)]. At $T_s \geq 1100 \text{ }^\circ\text{C}$ [“ $00l$ & $hh0$ ” region, squares in Fig. 1(a) and the top XRD pattern in Fig. 1(b)], $00l$ and $hh0$ preferential orientations were observed, which is similar to that observed for high- T_s growth of $\text{BaFe}_2\text{As}_2:\text{Co}$.^[17] A weak Fe 002 peak is observed in the XRD patterns. We confirmed that impurity Fe particles segregated in the bulk regions of the films, not at

the film–substrate interface (see Supplementary Figures S1(a) and (b) for the cross-sectional bright-field STEM image and EDXS spectra)^[18], sharply different from the result of BaFe₂As₂:Co films grown by PLD using a KrF excimer laser^[19]. In the latter report, the Fe impurity is epitaxially grown at the interface. However, similar segregation in the bulk region is observed also in BaFe₂As₂:Co epitaxial films fabricated using a Nd:YAG laser as an excitation source [S1(c) and (d)]^[18].

Based on these results, we concluded that the optimum T_s for epitaxial growth of BaFe₂As₂:P is ~1050 °C. The chemical composition of the film, as determined by EPMA, was Ba: Fe: As: P = 19.7: 41.5: 30.3: 8.5 [i.e., P/(As + P) = 22%], indicating that the P doping level was lower than the nominal composition of the PLD target [P/(As + P) = 30%]. The lattice parameters of the film were $a = 3.95 \text{ \AA}$ and $c = 12.830 \text{ \AA}$, which differ slightly from those of a single crystal with the same chemical composition ($a = 3.94 \text{ \AA}$ and $c = 12.89 \text{ \AA}$)^[20]. This result implies that a tensile strain in the ab plane is introduced into the epitaxial film because of the larger in-plane lattice parameter of the MgO substrate ($a = 4.21 \text{ \AA}$).

The surface morphology of the film grown at the optimum T_s , as observed by AFM, shows that the film grows via spiral-island growth and has a smooth surface with the step height corresponding to half of the c -axis length [Fig. 1(d)]. Note that there are few droplets and pit structures, although these are often observed in BaFe₂As₂:Co epitaxial films.^[21] These results would originate from the higher T_s growth (1050 °C) than that of BaFe₂As₂:Co epitaxial films (800–850 °C),^[17] which promotes the migration of deposition precursors and reconstruction of their structure at the growing surface. Such an atomically flat surface would be useful for future applications such as multilayer

junction devices.

Figure 1(e) shows ρ as a function of T for a $\text{BaFe}_2\text{As}_2\text{:P}$ epitaxial film grown at the optimum $T_s = 1050$ °C. A sharp superconducting transition at $T_c = 26.5$ K was observed with a small transition width of $\Delta T_c = 1.5$ K, which is consistent with the slightly underdoped P-concentration determined by EPMA [$\text{P}/(\text{As} + \text{P}) = 22\%$]; however, this T_c is 15 K higher than that of a single crystal with the same P concentration and is comparable to that of a 27% P-doped single crystal.^[22] As mentioned above, a tensile strain in the ab plane is introduced into the $\text{BaFe}_2\text{As}_2\text{:P}$ epitaxial films, which suggests that the effect of the tensile strain is opposite to an optimally doped $\text{BaFe}_2\text{As}_2\text{:Co}$ epitaxial film because a tensile strain decreases T_c for $\text{BaFe}_2\text{As}_2\text{:Co}$ ^[23]. On the other hand, it was recently reported that a tensile strain in a $\text{BaFe}_2\text{As}_2\text{:P}$ epitaxial film shifts its optimum doping level to an underdoped region^[24]. Thus, this result would be understood that the tensile strain shifts the optimum doping level to an underdoped region and the T_c of the present underdoped ($\text{P}/(\text{As} + \text{P}) = 22\%$) $\text{BaFe}_2\text{As}_2\text{:P}$ epitaxial films were enhanced.

After optimizing the T_s , the growth rate was varied with the T_s held at the optimum $T_s = 1050$ °C. As seen in Fig. 1(f), the rocking-curve FWHMs of $\Delta\omega$ and $\Delta\phi$ remain almost constant at $\sim 0.5^\circ$ for a growth rate ranging from 2.1 to 3.9 Å/s. This trend is different from that for $\text{BaFe}_2\text{As}_2\text{:Co}$ epitaxial films,^[25] where low growth rates such as 2.1 Å/s led to large $\Delta\omega$ and $\Delta\phi$ (FWHM $\sim 1^\circ$). This finding means that $\text{BaFe}_2\text{As}_2\text{:P}$ films may be grown over a wider range of growth rates, a result that is also attributed to the higher optimum T_s .

Next, we discuss anisotropy in transport J_c . For several growth rates, Fig. 2 shows

angular dependence of J_c for BaFe₂As₂:P epitaxial films grown at the optimum T_s . The data show that J_c increases with decreasing growth rate over the entire range of θ_H . This result is attributed to the improvement in the self-field J_c ; namely, at 12 K, the self-field J_c increased from 2.70 to 5.14 MA/cm² as the growth rate decreased from 3.9 to 2.2 Å/s. All the films exhibit intrinsic J_c peaks at $\theta_H = 90^\circ$ ($H // ab$), which is in agreement with the results for the film grown at the higher growth rate of 5.0 Å/s.^[7] The present films, however, exhibit additional J_c peaks at $\theta_H = 0^\circ$ ($H // c$). The value of J_c at $\theta_H = 0^\circ$ ($J_c^{H//c}$) increases with decreasing growth rate, then it exceeds J_c at $\theta_H = 90^\circ$ ($J_c^{H//ab}$) at the growth rate of 2.2 Å/s. These results indicate that vortex-pinning centers along the c -axis are introduced into BaFe₂As₂:P epitaxial films when these films are grown at a lower growth rate. Note that the J_c peak at $\theta_H = 0^\circ$ becomes larger and sharper upon decreasing the growth rate, which averages out the angle dependence of J_c and contributes to the highly isotropic property. These results indicate that the vortex-pinning properties and anisotropy of BaFe₂As₂:P epitaxial films can be controlled by tuning the growth rate.

Figure 3(a) compares the dependence of $J_c^{H//ab}$ (closed symbols) and $J_c^{H//c}$ (open symbols) at 4 K for BaFe₂As₂:P epitaxial film grown at the optimum T_s (1050 °C) and growth rate (2.2 Å/s) with what is found for other iron-based superconductor epitaxial films exhibiting high J_c . The self-field J_c of the optimally grown BaFe₂As₂:P epitaxial film was over 7 MA/cm², which is comparable to the best results recently reported,^[8] and a high $J_c^{H//ab}$ of over 1 MA/cm² was maintained even at 9 T. It would be noteworthy the value of $J_c^{H//ab}$ obtained at 9 T = 1.1 MA/cm² (corresponding to a pinning force of 99 GN/m³) is the highest obtained for iron-based superconductor thin films, as shown in Fig. 3(a).^[26–32] Moreover, at 9 T, $J_c^{H//c}$ is 0.8 MA/cm² and the pinning force is 72 GN/m³.

These values are higher than the previously reported ones, including those for 122-type compounds [e.g., BaFe₂As₂:P films with artificial pinning centers created by BaZrO₃ nanoparticles^[26] and oxygen-rich BaFe₂As₂/BaFe₂As₂:Co superlattice (SL) films^[28]] and conventional alloy superconducting wires (Nb-Ti,^[33] Nb₃Sn,^[34] and MgB₂^[35]).

Figure 3(b) compares the J_c anisotropy of the BaFe₂As₂:P epitaxial film with the J_c of other 122-type films^[7,26,28,29] in similar ranges of H and T . The BaFe₂As₂:P epitaxial film obtained in this study exhibited a lower anisotropy than those of BaFe₂As₂:P^[7] and BaFe₂As₂:Co/Fe buffer.^[29] Moreover, the anisotropy obtained is much lower than that of the SL thin films,^[28] and is comparable to that of the BaFe₂As₂:P films with artificial pinning centers created by BaZrO₃ nanoparticles.^[26]

As discussed above, the strong vortex pinning and the isotropic J_c properties were achieved by decreasing the growth rate for the BaFe₂As₂:P epitaxial films. Therefore, we investigate the origin of the pinning centers by microstructure analysis. Figures 4(a) and 4(b) show cross-sectional bright-field STEM images of BaFe₂As₂:P epitaxial films grown at 2.2 and 3.9 Å/s, respectively. Although small island structures (~ 20 nm in lateral size) rich in oxygen are periodically found at the heterointerface in the film grown at 2.2 Å/s, as indicated by the slanted black arrows, sharp heterointerfaces without a reaction layer were observed throughout the region. Other planar or line defects in the ab plane, such as stacking faults, were not detected. However, as indicated by the vertical white arrows in Fig. 4, many vertical defects, which occur at a higher density compared with that found for BaFe₂As₂:Co films,^[36] are observed in the STEM images. The number of defects did not significantly differ between the BaFe₂As₂:P films grown at 2.2 Å/s and 3.9 Å/s, but the shape and microstructure of the defects did differ. Most of the defects in the film grown at 2.2 Å/s start appearing at midthickness and are

oriented parallel to the c -axis, which would be assigned to vertical dislocations. However, most of the defects in the film grown at 3.9 \AA/s originate at the heterointerface just at the substrate surface and are tilted with respect to the c -axis. Such defects could be induced by lateral growth of the epitaxial domains. These results suggest that the defects in the film grown at 3.9 \AA/s are domain boundaries that initiate at the onset of film growth. This difference in the structure of the defects would correspond to the results of Fig. 2: against a magnetic field with $\theta_H = 0^\circ$, the vertical dislocations would pin vortices more strongly than the tilted domain boundaries, resulting in the sharper peak near $\theta_H = 0^\circ$ for films grown at 2.2 \AA/s and the broad peak near $\theta_H = 0^\circ$ for films grown at 3.9 \AA/s .

The STEM-EDXS line scans [Figs. 4(c) and 4(d)] show that the chemical composition of the defects is the same as that of the matrix region in the film and that the impurity oxygen concentration in the thin film is less than the detection limit of EDXS. We performed the EDXS line scans for six other vertical dislocations and nine domain boundaries, and obtained the same results. These results indicate that the defects are not an impurity phase such as BaFeO_2 ,^[37] but may be edge or threading dislocations and/or domain boundaries. The defect sizes are estimated to be $\sim 4 \text{ nm}$ laterally and roughly double of the superconducting coherence length in the ab plane of $\text{BaFe}_2\text{As}_2\text{:P}$ at 4 K ,^[7] which is consistent because such size defects effectively serve as vortex-pinning centers.

In summary, a high-self-field J_c of 7 MA/cm^2 was obtained for $\text{BaFe}_2\text{As}_2\text{:P}$ epitaxial films and a high J_c of over 1 MA/cm^2 was maintained even with an applied magnetic field of 9 T . This J_c value at 9 T is the highest value obtained so far for iron-based

superconductor thin films. In addition, a highly isotropic high J_c performance was obtained by decreasing the film growth rate, which introduced vertical dislocations along the c -axis that served as strong vortex-pinning centers.

Acknowledgment

This study was supported by the Japan Society for the Promotion of Science (JSPS), Japan, through the “Funding Program for World-Leading Innovative R&D on Science and Technology (FIRST Program)” and the Ministry of Education, Culture, Sports, Science and Technology (MEXT) Element Strategy Initiative to Form Core Research Center. H. Hiramatsu was also supported by a JSPS Grant-in-Aid for Young Scientists (A) Grant Number 25709058 and a JSPS Grant-in-Aid for Scientific Research on Innovative Areas “Nano Informatics” Grant Number 25106007.

References

1. Y. Kamihara, T. Watanabe, M. Hirano, and H. Hosono, *J. Am. Chem. Soc.* 130, 3296 (2008).
2. Z. -A. Ren, W. Lu, J. Yang, W. Yi, X. -L. Shen, Z. -C. Li, G. -C. Che, X. -L. Dong, L. -L. Sun, F. Zhou, and Z. -X. Zhao, *Chin. Phys. Lett.* 25, 2215 (2008).
3. F. Hunte, J. Jaroszynski, A. Gurevich, D.C. Larbalestier, R. Jin, A.S. Sefat, M.A. McGuire, B.C. Sales, D.K. Christen, and D. Mandrus, *Nature* 453, 903 (2008).
4. A. Yamamoto, J. Jaroszynski, C. Tarantini, L. Balicas, J. Jiang, A. Gurevich, D.C. Larbalestier, R. Jin, A.S. Sefat, M.A. McGuire, B.C. Sales, D.K. Christen, and D.

- Mandrus, *Appl. Phys. Lett.* 94, 062511 (2009).
5. T. Katase, Y. Ishimaru, A. Tsukamoto, H. Hiramatsu, T. Kamiya, K. Tanabe, and H. Hosono, *Nat. Commun.* 2, 409 (2011).
6. H. Hiramatsu, T. Katase, T. Kamiya, and H. Hosono, *J. Phys. Soc. Jpn.* 81, 011011 (2012).
7. M. Miura, S. Adachi, T. Shimode, K. Wada, A. Takemori, N. Chikumoto, K. Nakao, and K. Tanabe, *Appl. Phys. Express* 6, 093101 (2013).
8. A. Sakagami, T. Kawaguchi, M. Tabuchi, T. Ujihara, Y. Takeda, and H. Ikuta, *Physica C* 494, 181 (2013).
9. S. Lee, J. Jiang, Y. Zhang, C.W. Bark, J.D. Weiss, C. Tarantini, C.T. Nelson, H.W. Jang, C.M. Folkman, S.H. Baek, A. Polyanskii, D. Abraimov, A. Yamamoto, J.W. Park, X.Q. Pan, E.E. Hellstrom, D.C. Larbalestier, and C.B. Eom, *Nat. Mater.* 9, 397 (2010).
10. T. Katase, H. Hiramatsu, T. Kamiya, and H. Hosono, *Appl. Phys. Express* 3, 063101 (2010).
11. B. Maierov, T. Katase, I.O. Usov, M. Weigand, L. Civale, H. Hiramatsu, and H. Hosono, *Phys. Rev. B* 86, 094513 (2012).
12. C. J. van der Beek, M. Konczykowski, S. Kasahara, T. Terashima, R. Okazaki, T. Shibauchi, and Y. Matsuda, *Phys. Rev. Lett.* 105, 267002 (2010).
13. S. Demirdiř, Y. Fasano, S. Kasahara, T. Terashima, T. Shibauchi, Y. Matsuda, M. Konczykowski, H. Pastoriza, and C.J. van der Beek, *Phys. Rev. B* 87, 094506 (2013).
14. J.L. MacManus-Driscoll, S.R. Foltyn, Q.X. Jia, H. Wang, A. Serquis, L. Civale, B.

- Maierov, M.E. Hawley, M.P. Maley, and D.E. Peterson, *Nat. Mater.* 3, 439 (2004).
15. K. Matsumoto and P. Mele, *Supercond. Sci. Technol.* 23, 014001 (2010).
16. L. Fang, Y. Jia, C. Chaparro, G. Sheet, H. Claus, M.A. Kirk, A.E. Koshelev, U. Welp, G.W. Crabtree, W.K. Kwok, S. Zhu, H.F. Hu, J.M. Zuo, H.-H. Wen, and B. Shen, *Appl. Phys. Lett.* 101, 012601 (2012).
17. T. Katase, H. Hiramatsu, T. Kamiya, and H. Hosono, *Supercond. Sci. Technol.* 25, 084015 (2012).
18. See supplementary material at [<http://dx.doi.org/10.1063/1.4875956>] for the cross-sectional STEM image and EDXS spectra.
19. K. Iida, J. Hänisch, T. Thersleff, F. Kurth, M. Kitzun, S. Haindl, R. Hühne, L. Schultz, and B. Holzapfel, *Phys. Rev. B* 81, 100507 (2010).
20. S. Kasahara, T. Shibauchi, K. Hashimoto, K. Ikada, S. Tonegawa, R. Okazaki, H. Shishido, H. Ikeda, H. Takeya, K. Hirata, T. Terashima, and Y. Matsuda, *Phys. Rev. B* 81, 184519 (2010).
21. T. Katase, H. Hiramatsu, H. Yanagi, T. Kamiya, M. Hirano, and H. Hosono, *Solid State Commun.* 149, 2121 (2009).
22. H. Shishido, A.F. Bangura, A.I. Coldea, S. Tonegawa, K. Hashimoto, S. Kasahara, P.M.C. Rourke, H. Ikeda, T. Terashima, R. Settai, Y. Ōnuki, D. Vignolles, C. Proust, B. Vignolle, A. McCollam, Y. Matsuda, T. Shibauchi, and A. Carrington, *Phys. Rev. Lett.* 104, 057008 (2010).
23. K. Iida, J. Hänisch, R. Hühne, F. Kurth, M. Kitzun, S. Haindl, J. Werner, L.

- Schultz, and B. Holzapfel, *Appl. Phys. Lett.* 95, 192501 (2009).
24. T. Kawaguchi, A. Sakagami, Y. Mori, M. Tabuchi, T. Ujihara, Y. Takeda, and H. Ikuta, *Supercond. Sci. Technol.* 27, 065005 (2014).
25. H. Hiramatsu, H. Sato, T. Katase, T. Kamiya and H. Hosono, to be published in *Appl. Phys. Lett.*
26. M. Miura, B. Maiorov, T. Kato, T. Shimode, K. Wada, S. Adachi, and K. Tanabe, *Nat. Commun.* 4, 2499 (2013).
27. K. Iida, J. Hänisch, C. Tarantini, F. Kurth, J. Jaroszynski, S. Ueda, M. Naito, A. Ichinose, I. Tsukada, E. Reich, V. Grinenko, L. Schultz, and B. Holzapfel, *Sci. Rep.* 3, 2139 (2013).
28. S. Lee, C. Tarantini, P. Gao, J. Jiang, J.D. Weiss, F. Kametani, C.M. Folkman, Y. Zhang, X.Q. Pan, E.E. Hellstrom, D.C. Larbalestier, and C.B. Eom, *Nat. Mater.* 12, 392 (2013).
29. K. Iida, S. Haindl, T. Thersleff, J. Hänisch, F. Kurth, M. Kitzun, R. Hühne, I. Mönch, L. Schultz, B. Holzapfel, and R. Heller, *Appl. Phys. Lett.* 97, 172507 (2010).
30. S. Trommler, J. Hänisch, V. Matias, R. Hühne, E. Reich, K. Iida, S. Haindl, L. Schultz, and B. Holzapfel, *Supercond. Sci. Technol.* 25, 084019 (2012).
31. V. Braccini, S. Kawale, E. Reich, E. Bellingeri, L. Pellegrino, A. Sala, M. Putti, K. Higashikawa, T. Kiss, B. Holzapfel, and C. Ferdeghini, *Appl. Phys. Lett.* 103, 172601 (2013).
32. H. Hiramatsu, T. Katase, Y. Ishimaru, A. Tsukamoto, T. Kamiya, K. Tanabe, and H.

Hosono, *Mater. Sci. Eng. B* 177, 515 (2012).

33. L.D. Cooley, P.J. Lee, and D.C. Larbalestier, *Phys. Rev. B* 53, 6638 (1996).

34. A. Godeke, *Supercond. Sci. Technol.* 19, R68 (2006).

35. C.G. Zhuang, S. Meng, H. Yang, Y. Jia, H.H. Wen, X.X. Xi, Q.R. Feng, and Z.Z. Gan, *Supercond. Sci. Technol.* 21, 082002 (2008).

36. H. Sato, T. Katase, W.N. Kang, H. Hiramatsu, T. Kamiya, and H. Hosono, *Phys. Rev. B* 87, 064504 (2013).

37. Y. Zhang, C.T. Nelson, S. Lee, J. Jiang, C.W. Bark, J.D. Weiss, C. Tarantini, C.M. Folkman, S.-H. Baek, E.E. Hellstrom, D.C. Larbalestier, C.-B. Eom, and X. Pan, *Appl. Phys. Lett.* 98, 042509 (2011).

Figure captions

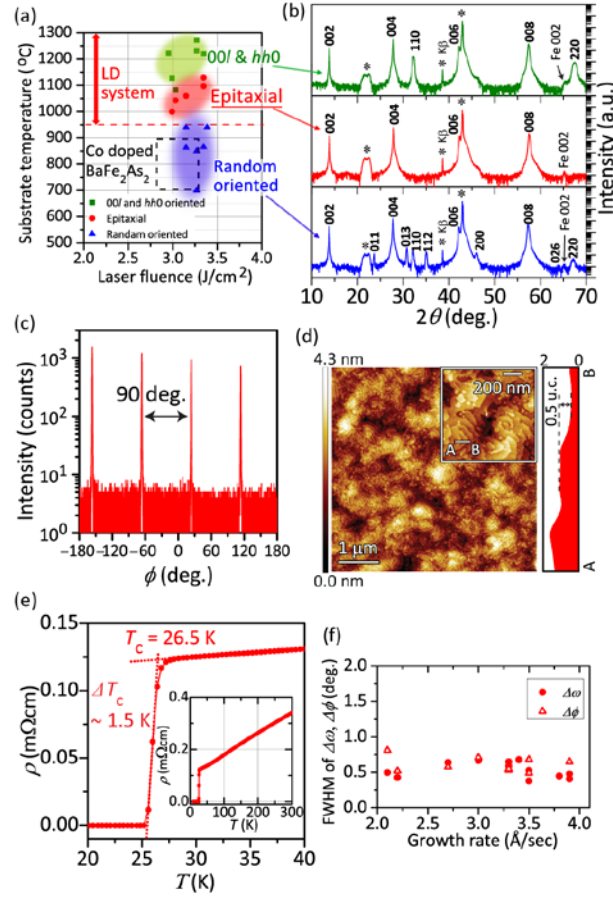


Fig. 1. (Color online) Growth of BaFe₂As₂:P films and structural and electrical properties of the epitaxial film. (a) Relationship between growth condition (substrate temperature T_s and laser fluence) and crystallographic orientation of BaFe₂As₂:P films. Three regions with different orientation structures obtained with different T_s values are shown. The dashed square region shows the optimum condition for epitaxial growth of BaFe₂As₂:Co.^[17] (b) Typical XRD patterns, measured in Bragg-Brentano configuration, of BaFe₂As₂:P thin films for the three T_s regions in panel (a). (c) In-plane ϕ scan of the 200 diffractions of the BaFe₂As₂:P thin film grown at the optimum T_s . (d) AFM scan showing surface morphology of BaFe₂As₂:P film grown at the optimum T_s . Upper-right inset shows a magnified image. A cross-sectional profile along the horizontal line A-B in the inset is shown to the right (“0.5 u.c.” denotes the half size of the c -axis unit-cell length). (e) Resistivity as a function of temperature for BaFe₂As₂:P thin film grown at the optimum T_s . Inset shows data from 10 to 300 K. (f) Dependence of FWHM of $\Delta\omega$ and $\Delta\phi$ on growth rate of BaFe₂As₂:P films grown at the optimum T_s .

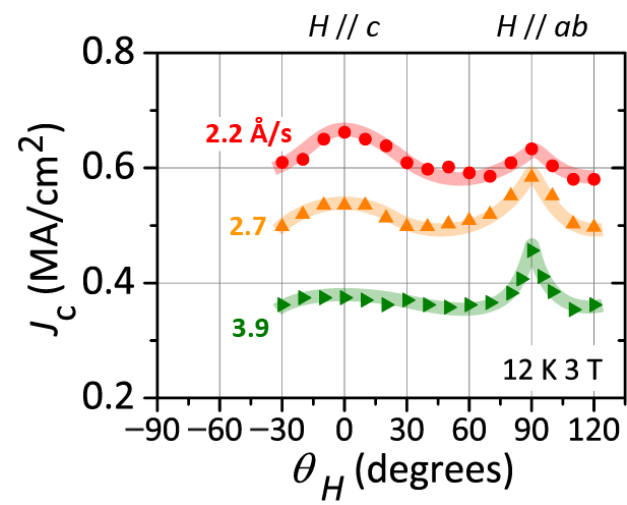


Fig. 2 (Color online) Critical current density J_c as a function of angle of applied magnetic field θ_H for BaFe₂As₂:P epitaxial films grown at three growth rates, with $\mu_0 H = 3$ T and $T = 12$ K.

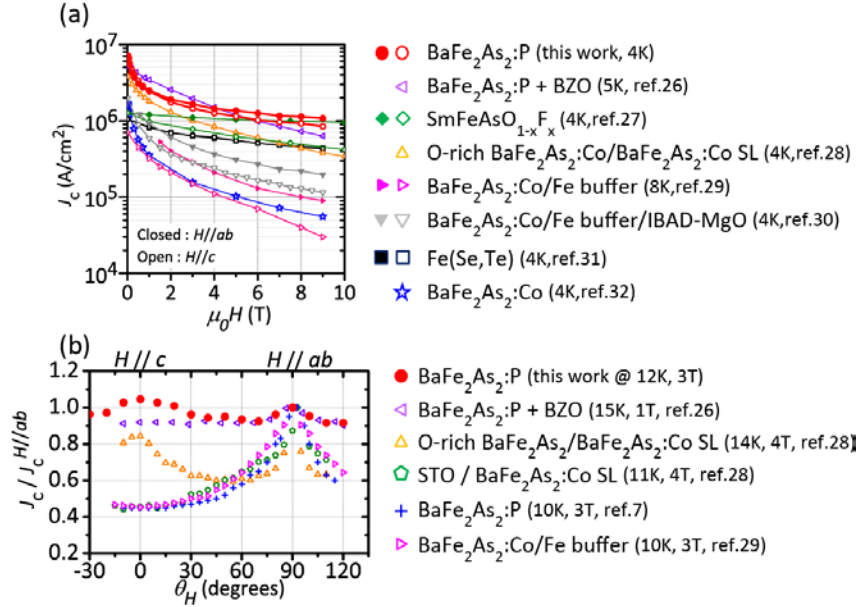


Fig. 3. (Color online) (a) Critical current density J_c as a function of magnetic-field H for BaFe₂As₂:P epitaxial film grown at the optimum T_s (1050 °C) and growth rate (2.2 Å/s) (circles). Open and closed symbols show the data obtained by applying $H // c$ and $H // ab$, respectively. (b) Dependence of J_c (normalized to $J_c^{H//ab}$) on angle of external magnetic field θ_H for BaFe₂As₂:P epitaxial film at 12 K and 3 T (circles). Also shown for comparison are the data for BaFe₂As₂:P + 3 mol% BaZrO₃ nanoparticles (left-pointing triangles),^[26] SmFeAsO_{1-x}F_x (diamonds),^[27] O-rich BaFe₂As₂/BaFe₂As₂:Co superlattice (SL) (triangles),^[28] STO/BaFe₂As₂:Co SL (pentagons),^[28] BaFe₂As₂:Co/Fe buffer (right-pointing triangles),^[29] BaFe₂As₂:P (crosses),^[7] BaFe₂As₂:Co/Fe/IBAD-MgO (inverse triangles),^[30] Fe(Se,Te) (squares).^[31] and BaFe₂As₂:Co (stars).^[32]

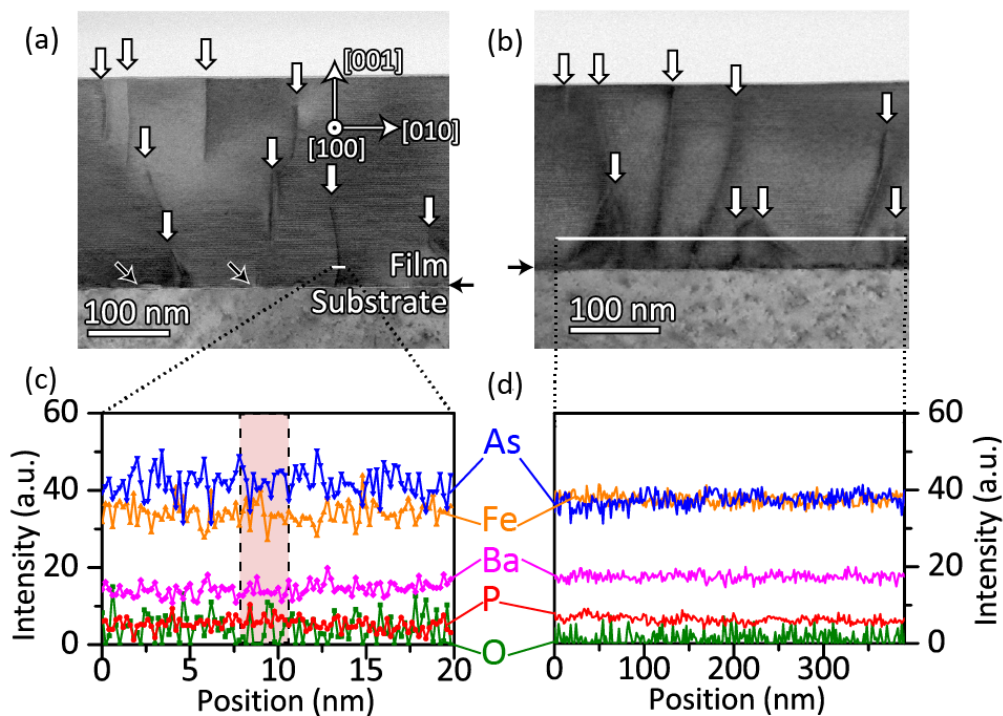


Fig. 4. (Color online) Cross-sectional bright-field STEM images of BaFe₂As₂:P epitaxial films grown at the growth rates (a) 2.2 Å/s and (b) 3.9 Å/s. The horizontal black arrow on the side of each figure indicates the heterointerface between the substrate and the BaFe₂As₂:P epitaxial film. The vertical white arrows indicate the vertical defects, and the slanted black arrows indicate oxygen-rich island structures. Panels (c) and (d) show the results of an STEM-EDXS line scan along the horizontal line shown in panels (a) and (b), respectively. The dashed shaded region in panel (c) corresponds to the vertical defect in panel (a).

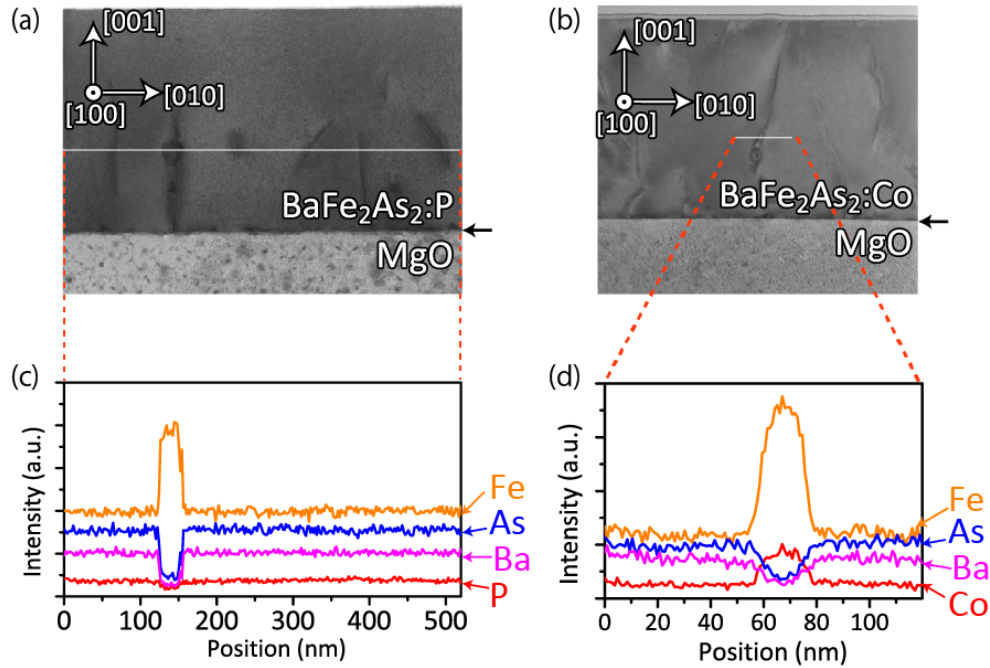
Supplementary material for “ High critical-current density with less anisotropy in $\text{BaFe}_2(\text{As,P})_2$ epitaxial thin films: effect of intentionally grown c -axis vortex-pinning centers”

Hikaru Sato¹, Hidenori Hiramatsu^{1,2}, Toshio Kamiya^{1,2}, and Hideo Hosono^{1,2,3}

1: *Materials and Structures Laboratory, Tokyo Institute of Technology, Mailbox R3-1, 4259 Nagatsuta-cho, Midori-ku, Yokohama 226-8503, Japan*

2: *Materials Research Center for Element Strategy, Tokyo Institute of Technology, Mailbox S2-16, 4259 Nagatsuta-cho, Midori-ku, Yokohama 226-8503, Japan*

3: *Frontier Research Center, Tokyo Institute of Technology, Mailbox S2-13, 4259 Nagatsuta-cho, Midori-ku, Yokohama 226-8503, Japan*



Supplementary FIG. S1. Cross-sectional bright-field STEM images of $\text{BaFe}_2\text{As}_2:\text{P}$ (a) and $\text{BaFe}_2\text{As}_2:\text{Co}$ (b)^[Ref] epitaxial films. Horizontal arrows indicate the heterointerfaces between the films and MgO substrates. Panels (c) and (d) show the results of EDXS line-scans along the white horizontal lines in panels (a) and (b), respectively.

[Ref] T. Katase, H. Hiramatsu, T. Kamiya, and H. Hosono, *Supercond. Sci. Technol.* **25**, 084015 (2012).